On the Observability and the Observer Design of Differential Pneumatic Pistons

Marco A. Arteaga–Pérez*
Departamento de Control y Robótica
DIE. Facultad de Ingeniería
Universidad Nacional
Autónoma de México
México, D. F., 04510, México
E–mail: marteagp@unam.mx

Alejandro Gutiérrez–Giles
Departamento de Control y Robótica
DIE. Facultad de Ingeniería
Universidad Nacional
Autónoma de México
México, D. F., 04510, México
E–mail: alejandrogilesg@yahoo.com.mx

Jens Weist
Volkswagen AG, Letter Box 1399/5
D–38436, Wolfsburg, Germany
E–mail: jens@jensweist.de

In this paper, an observability analysis for differential pneumatic pistons is presented, together with observer design and implementation. To avoid as much as possible the knowledge of the system model parameters, the GPI (Generalized Proportional Integral) approach is employed for the estimation of unmeasured variables. Experimental results show the good performance of the proposed scheme.

1 Introduction

The attractiveness of pneumatic systems lies on their cleanness, low prices, excellent weight to force ratio and easy assembling. Industrial applications for this kind of devices are wide, for instance in food production, robotic manipulators or oil industry with flammable environments. Therefore, it is important to design controllers capable of reaching the same performance as for electric or hydraulic actuators.

The main control goals for differential pneumatic devices are displacement and force tracking of the piston. In either case it is necessary to regulate the mass flow entering into the two chambers. Depending on the actuator, it may be controlled by many kinds of valves, like simple ON/OFF or proportional arrangements. The last ones generate mass flows which depend on the control input voltage.

While there are many works regarding the designed and implementation of different control strategies for pneumatic systems (*e. g.* [1–8]), there are fewer regarding research on observer design. For instance, Bigras and Khayati [9] developed a nonlinear observer for pressure estimation of a class of pneumatic systems where the cylinder connection ports comprise a non negligible restriction. Only simulation results are presented. In [10] the design of a sliding mode control law is proposed for which only the measurement of one chamber pressure of a differential cylinder is necessary, while the other one is estimated online by means of an observer. Although the approach is simple, it turns out to be very sensitive to friction effects. In [11, 12] a nonlinear observability analysis is developed to find out whether it is possible to design a control law based only on the piston position, y, while pressure measurements are eliminated via observer design. The results show that local observability is lost in several regions of the state space, in particular when $\dot{y} = 0$. In [13] the design of two Lyapunov–based nonlinear pressure observers is introduced. The approach is successfully tested experimentally. However, the implementation requires many information about the pneumatic system, which represents a disadvantage.

In this paper, an observability analysis for differential pneumatic pistons is presented. Based on the results, linear observers are implemented for the estimation of one chamber pressure and the piston velocity. To avoid the computation of the high nonlinear dynamics of the piston chambers, the GPI (*Generalized Proportional Integral*) approach is employed [14, 15]. The result is an observer that does not need the mass flow chamber dynamics at all. Experimental results show the good performance of the proposed scheme.

The paper is organized as follows: in Section 2 the dynamic model for differential pneumatic pistons is given. Section 3 carries out the observability analysis and Section 4 describes the observer design. Section 5 shows the experimental results, while Section 6 gives some conclusions.

*Corresponding author.

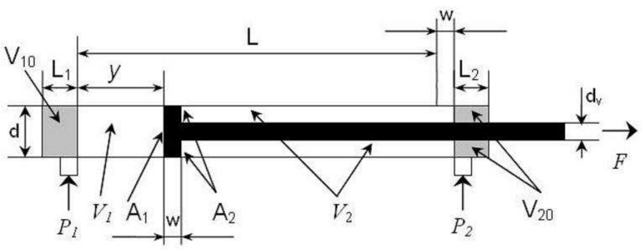

Fig. 1. Differential pneumatic piston structure

2 Differential pneumatic pistons

2.1 Dynamic model

Figure 1 depicts the general structure of a differential pneumatic piston, where L [m] is the maximal piston displacement, y [m] is the piston position and $\dot{y}$ $[\frac{\mathrm{m}}{\mathrm{s}}]$ is the corresponding velocity. For $i = 1, 2$, L_i [m] is the width of the dead zone of chamber i, d [m] is the piston diameter, A_i $[\mathrm{m}^2]$ is the cross section area of piston chamber i, V_i $[\mathrm{m}^3]$ is the volume in chamber i, V_{i0} $[\mathrm{m}^3]$ is the dead volume of chamber i including tubes, d_v [m] is the piston rod diameter, w [m] is the piston width, p_i [Pa] is the pressure of chamber i. Finally, F [N] is the applied force.

The system state is usually defined as

$$\mathbf{x} = \begin{bmatrix} x_1 \\ x_2 \\ x_3 \\ x_4 \end{bmatrix} \triangleq \begin{bmatrix} y \\ \dot{y} \\ p_1 \\ p_2 \end{bmatrix}. \tag{1}$$

Model development can be found in many works [16–18]. In the following we do a sketch of the procedure. Basically, Newton's second law and the first law of thermodynamics for adiabatic processes are employed. As a matter of fact, two subsystems can be distinguished. The mechanical part whose dynamics is given by

$$\dot{x}_1 = x_2 \tag{2}$$

$$\dot{x}_2 = \frac{A_1}{M}x_3 - \frac{A_2}{M}x_4 - \frac{A_1 - A_2}{M}p_{\mathrm{atm}} - \frac{F_\mathrm{V}}{M}x_2, \tag{3}$$

and the pneumatic components described by

$$\dot{x}_3 = \frac{\gamma}{V_{10} + A_1 x_1}\left(RT\dot{m}_1(x_3, u) - x_2 x_3 A_1\right) \tag{4}$$

$$\dot{x}_4 = \frac{\gamma}{V_{20} + A_2(L - x_1)}\left(RT\dot{m}_2(x_4, u) - x_2 x_4 A_2\right), \tag{5}$$

where p_{atm} [Pa] is the atmospheric pressure, M [kg] is the piston mass, F_V $[(\mathrm{N}\cdot\mathrm{m})/\mathrm{s}]$ is the viscous friction coefficient, γ is the adiabatic index, R $[\mathrm{J}/(\mathrm{kg}\cdot\mathrm{K})]$ is the air gas constant, T [K] is the temperature, u [V] is the input voltage and $\dot{m}_i$ $[\mathrm{kg/s}]$ is the mass flow chamber i, $i = 1, 2$, given by

$$\dot{m}_1 = C(u)\overline{\gamma}_1(x_3) \tag{6}$$

$$\triangleq C(u)\begin{cases} \rho_0 p_\mathrm{s}\sqrt{1 - \left(\dfrac{\left(\dfrac{x_3}{p_\mathrm{s}} - b\right)}{1 - b}\right)^2} & u \geq 0 \text{ and } \dfrac{x_3}{p_\mathrm{s}} \geq b \\ \rho_0 p_\mathrm{s} & u \geq 0 \text{ and } \dfrac{x_3}{p_\mathrm{s}} < b \\ \rho_0 x_3 & u < 0 \end{cases}$$

and

$$\dot{m}_2 = -C(u)\overline{\gamma}_2(x_4) \tag{7}$$

$$\triangleq -C(u)\begin{cases} \rho_0 x_4 & u > 0 \\ \rho_0 p_\mathrm{s}\sqrt{1 - \left(\dfrac{\left(\dfrac{x_4}{p_\mathrm{s}} - b\right)}{1 - b}\right)^2} & u \leq 0 \text{ and } \dfrac{x_4}{p_\mathrm{s}} \geq b \\ \rho_0 p_\mathrm{s} & u \leq 0 \text{ and } \dfrac{x_4}{p_\mathrm{s}} < b \end{cases}$$

where ρ_0 $\left[\mathrm{kg/m^3}\right]$ is the air density, p_s [Pa] is the supply pressure, b is the critical pressure ratio and $C(u)$ [kg/s] is the mass flow function.

Remark 2.1.
The input voltage u usually takes values from 0V to +10V, but in (6)–(7) it is considered that $u \in (-5, +5)V$ while a constant value $V_{\mathrm{offset}} \approx 5V$ is added for implementation. △

3 Observability analysis

In this section, an observability analysis of the state of system (2)–(5) is carried out. Our main goal is to design an observer with the minimal number of sensors. Note that usually three of them are employed, namely one for the displacement (y) and two for the pressures in the chambers of the piston (p_1 and p_2), while the derivative $\dot{y}$ may be computed numerically. The question is whether only one or at most two sensors can be used. Based on Table 1, we consider that there are seven cases of interest. In order to simplify the observability analysis, we follow the well–known criterion that the state is observable as long as it can be written as a function of the measured variables, the different inputs, and a finite number of their corresponding derivatives [19].

3.1 Case 1: x_1 (y) available

Clearly, x_2 can be gotten just by computing the derivative of x_1. However, it is not posible to get x_3 from (4) or x_4 from (5) only as a function of x_1 and its derivatives because both $\dot{x}_3$ and $\dot{x}_4$ are involved, respectively. An attempt to eliminate them by computing $\ddot{x}_2$ from (3) and substituting $\dot{x}_3$ and $\dot{x}_4$ would just lead to a nonlinear relationship between x_3 and x_4. Thus, we can conclude that the state is not observable if only x_1 is available. It is worthy to note that by applying the observability analysis described in [20], in [11, 12] the authors show that the state is observable only if $\dot{y} = x_2 \neq 0$. Clearly, this case is of little practical interest, since usually one has $\dot{y} = 0$ for some time intervals.

Case	Available			Non Available				Obs
1	y				$\dot{y}$	p_1	p_2	N
2		p_1		y	$\dot{y}$		p_2	N
3			p_2	y	$\dot{y}$	p_1		N
4	y	p_1			$\dot{y}$		p_2	Y
5	y		p_2		$\dot{y}$	p_1		Y
6		p_1	p_2	y	$\dot{y}$			N
7	y	p_1	p_2		$\dot{y}$			Y

Table 1. Complete Observability Analysis Scheme

3.2 Cases 2 and 3: x_3 (p_1) or x_4 (p_2) available

Consider that only p_1 is available. Then, the state will be observable if y (x_1), $\dot{y}$ (x_2) and p_2 (x_4) can be expressed as a function of p_1 and its derivatives. We begin with x_2. From (4) one gets

$$x_2 = \frac{RT\dot{m}_1(x_3,u)}{x_3 A_1} - \frac{\dot{x}_3(V_{10}+A_1x_1)}{\gamma x_3 A_1}. \tag{8}$$

As can be appreciated x_2 is a function of x_1, x_3, the input and their derivatives. An attempt to eliminate x_1 would consist in computing the derivative of (8) to use (3). However, x_1 does not disappear and, furthermore, x_4 arises as well. Clearly, there is therefore no way to write x_2 only as a function of x_3 and one can conclude that the state is not observable. Note that the same conclusion can be gotten if x_4 is available instead of x_3.

3.3 Cases 4 and 5: x_1 (y) and x_3 (p_1) or x_4 (p_2) available

For these cases, $x_2 = \dot{x}_1$. Suppose x_3 is available, so that we need to determine whether it is possible to write x_4 only as a function of x_1, x_3 and their derivatives. Directly from (3) it is

$$x_4 = \frac{A_1}{A_2}x_3 - \frac{A_1-A_2}{A_2}p_{\text{atm}} - \frac{F_V}{A_2}x_2 - \frac{M}{A_2}\dot{x}_2. \tag{9}$$

Based on (9) we can conclude that the state is observable. Alternatively, when x_4 is the available variable one gets

$$x_3 = \frac{A_2}{A_1}x_4 + \frac{A_1-A_2}{A_1}p_{\text{atm}} + \frac{F_V}{A_1}x_2 + \frac{M}{A_1}\dot{x}_2. \tag{10}$$

So, the state is also observable, as could have been expected.

3.4 Case 6: x_3 (p_1) and x_4 (p_2) available

As before, the goal is to write x_1 and x_2 as a function of only x_3, x_4, the input and their derivatives. By combining (4) and (5) one gets

$$x_1 = -\frac{\gamma}{A_2\dot{x}_4}\left(RT\dot{m}_2 - x_2x_4A_2\right) + \frac{V_{20}+A_2L}{A_2} \tag{11}$$

$$= \frac{\gamma}{A_1\dot{x}_3}\left(RT\dot{m}_1 - x_2x_3A_1\right) - \frac{V_{10}}{A_1},$$

so that x_2 can be obtained as

$$\begin{aligned} x_2 = {} & RT\frac{\dot{m}_1A_2\dot{x}_4 + \dot{m}_2A_1\dot{x}_3}{A_1A_2(x_4\dot{x}_3 + x_3\dot{x}_4)} \\ & - \frac{\dot{x}_3\dot{x}_4}{\gamma(x_4\dot{x}_3 + x_3\dot{x}_4)}\left(\frac{V_{10}}{A_1} + \frac{V_{20}+A_2L}{A_2}\right). \end{aligned} \tag{12}$$

By replacing (12) in (11) one gets

$$\begin{aligned} x_1 = {} & \frac{\gamma}{A_1\dot{x}_3}\Bigg(RT\dot{m}_1 - x_3A_1\Bigg(RT\frac{\dot{m}_1A_2\dot{x}_4 + \dot{m}_2A_1\dot{x}_3}{A_1A_2(x_4\dot{x}_3 + x_3\dot{x}_4)} \\ & - \frac{\dot{x}_3\dot{x}_4}{\gamma(x_4\dot{x}_3 + x_3\dot{x}_4)}\left(\frac{V_{10}}{A_1} + \frac{V_{20}+A_2L}{A_2}\right)\Bigg)\Bigg) - \frac{V_{10}}{A_1}, \end{aligned} \tag{13}$$

or

$$\begin{aligned} x_1 = {} & -\frac{\gamma}{A_2\dot{x}_4}\Bigg(RT\dot{m}_2 - x_4A_2\Bigg(RT\frac{\dot{m}_1A_2\dot{x}_4 + \dot{m}_2A_1\dot{x}_3}{A_1A_2(x_4\dot{x}_3 + x_3\dot{x}_4)} \\ & - \frac{\dot{x}_3\dot{x}_4}{\gamma(x_4\dot{x}_3 + x_3\dot{x}_4)}\left(\frac{V_{10}}{A_1} + \frac{V_{20}+A_2L}{A_2}\right)\Bigg)\Bigg) + \frac{V_{20}+A_2L}{A_2}. \end{aligned} \tag{14}$$

Clearly, the state is not observable if $\dot{x}_3 = 0$ and/or $\dot{x}_4 = 0$, *i. e.* if either p_1 or p_2 are constant.

3.5 Case 7: x_1 (y), x_3 (p_1) and x_4 (p_2) available

The state is trivially observable since, as usual, $x_2 = \dot{x}_1$.

4 Observer design

According to the results of Section 3, there are only three cases for the state of system (2)–(5) to be observable, namely when the position y (x_1) and the pressure p_1 (x_3) (or the pressure p_2 (x_4)) are available or when these three variables can be measured. In this section two observers will be designed for the first two options. As pointed out in [8], it is difficult to get an accurate dynamic model to represent the dynamics of the complete system (2)–(7), specially for equations (6)–(7). Thus, the less information employed for implementation the better. In this work we propose the use of the GPI (*Generalized Proportional Integral*) approach due to the flexibility of the design [15].

Suppose that x_1 and x_3 are available, while x_2 and x_4 are to be estimated, and rewrite (2)–(3) as

$$\dot{x}_1 = x_2 \tag{15}$$

$$\dot{x}_2 = \frac{A_1}{M}x_3 + z_1 - \frac{A_1-A_2}{M}p_{\text{atm}} - \frac{F_V}{M}x_2. \tag{16}$$

Note that (4) is not necessary since x_3 is measured, while x_4 is substituted by

$$z_1 \triangleq -\frac{A_2}{M}x_4 \qquad \Rightarrow \qquad x_4 = -\frac{M}{A_2}z_1. \tag{17}$$

Consider the following assumption [15].

Assumption 4.1. *For the variable z_1 in (17) it holds*

1. *z_1 and a finite number of its time derivatives, say p of them, are absolutely uniformly bounded.*
2. *z_1 can be expressed as*

$$z_1 = \sum_{i=0}^{p-1} a_i t^i + r(t) \tag{18}$$

with each a_i being a constant coefficient.

3. *The continuously updated residual term, $r(t)$, and its time derivatives in the instantaneous Taylor polynomial approximation of the signal z_1, are bounded. Note in particular that then $r^{(p)}$ is bounded.* △

Remark 4.1.
The definition of z_1 in (17) is aimed at avoiding the knowledge, and especially the employment, of (5) and (7). This is possible as long as Assumption 4.1 holds. △

Remark 4.2.
Assumption 4.1 may appear to be too restrictive, however, it should be taken into account that the following physical facts hold:

1. $p_{\text{atm}} \leq x_3, x_4 \leq p_{\text{s}}$.
2. $0 \leq x_1 \leq L$.
3. $\overline{\gamma}_1(x_3), \overline{\gamma}_2(x_4) \geq 0$ and bounded.
4. $C(u)$ is a continuous strictly increasing function with $C(0) = 0$.

Automatically Item 1. guarantees the boundedness of z_1. Items 2.–4. guarantee the boundedness of $\dot{x}_3, \dot{x}_4$ as long as x_2 ($\dot{y}$) is bounded. From a practical and physical point of view this can be expected. Thus, Assumption 4.1 is not really restrictive regarding the boundedness of z_1 and its derivatives. See [15] for full details about the interpretation of z_1. △

After Assumption 4.1, equations (15) and (16) can be rewritten as

$$\dot{x}_1 = x_2 \tag{19}$$
$$\dot{x}_2 = -ax_2 + bx_3 + z_1 + \overline{u} \tag{20}$$
$$\dot{z}_1 = z_2 \tag{21}$$
$$\vdots$$
$$\dot{z}_{p-1} = z_p = z_1^{(p-1)} \tag{22}$$
$$\dot{z}_p = r^{(p)}(t) = z_1^{(p)}, \tag{23}$$

where it has been conveniently set

$$a = \frac{F_{\text{V}}}{M} \tag{24}$$
$$b = \frac{A_1}{M} \tag{25}$$
$$\overline{u} = -\frac{A_1 - A_2}{M} p_{\text{atm}}. \tag{26}$$

Based on (19)–(23) and by defining

$$e = x_1 - \hat{x}_1, \tag{27}$$

the following linear observer can be introduced

$$\dot{\hat{x}}_1 = \hat{x}_2 + \lambda_{p+1} e - ae \tag{28}$$
$$\dot{\hat{x}}_2 = -a\dot{\hat{x}}_1 + bx_3 + \hat{z}_1 + \overline{u} + \lambda_p e \tag{29}$$
$$\dot{\hat{z}}_1 = \hat{z}_2 + \lambda_{p-1} e \tag{30}$$
$$\dot{\hat{z}}_2 = \hat{z}_3 + \lambda_{p-2} e \tag{31}$$
$$\vdots$$
$$\dot{\hat{z}}_{p-1} = \hat{z}_p + \lambda_1 e \tag{32}$$
$$\dot{\hat{z}}_p = \lambda_0 e. \tag{33}$$

System (19)–(23) in closed loop with the GPI observer given by (28)–(33) delivers the error dynamics

$$\dot{e} = e_2 - \lambda_{p+1} e + ae \tag{34}$$
$$\dot{e}_2 = -a\dot{e} + \tilde{z}_1 - \lambda_p e \tag{35}$$
$$\dot{\tilde{z}}_1 = \tilde{z}_2 - \lambda_{p-1} e \tag{36}$$
$$\dot{\tilde{z}}_2 = \tilde{z}_3 - \lambda_{p-2} e \tag{37}$$
$$\vdots$$
$$\dot{\tilde{z}}_{p-1} = \tilde{z}_p - \lambda_1 e \tag{38}$$
$$\dot{\tilde{z}}_p = r^{(p)}(t) - \lambda_0 e, \tag{39}$$

where $e_2 = x_2 - \hat{x}_2$ and $\tilde{z}_i = z_i - \hat{z}_i$, for $i = 1, \ldots, p$.

Theorem 4.1. *Suppose that Assumption 4.1 holds. Then for the error dynamics (34)–(39), the observation errors e, $\dot{e}$ and $\tilde{z}_1$ globally asymptotically tend to an arbitrary small neighborhood of the origin as long as the gains $\{\lambda_0, \lambda_1, \ldots, \lambda_{p+1}\}$ are chosen in such a manner that the polynomial*

$$\rho(s) = s^{p+2} + \lambda_{p+1} s^{p+1} + \cdots + \lambda_1 s + \lambda_0 \tag{40}$$

is Hurwitz with roots located sufficiently far into the left half of the complex plane. Furthermore, an estimate of $\hat{x}_4$ is given by

$$\hat{x}_4 = -\frac{M}{A_2} \hat{z}_1. \tag{41}$$

Proof

By combining (34)–(35) one gets

$$\ddot{e}+\lambda_{p+1}\dot{e}+\lambda_p e=\tilde{z}_1. \tag{42}$$

On the other hand, from (36)–(37) it is

$$\dddot{\tilde{z}}_1=\tilde{z}_3-\lambda_{p-2}e-\lambda_{p-1}\dot{e}. \tag{43}$$

Proceeding in the same way until reaching (39) results in

$$\tilde{z}_1^{(p)}=r^{(p)}(t)-\lambda_0 e-\cdots-\lambda_{p-1}e^{(p-1)}. \tag{44}$$

Then, one gets after (42) and (44)

$$e^{(p+2)}+\lambda_{p+1}e^{(p+1)}+\cdots+\lambda_0 e=r^{(p)}(t)=\frac{\mathrm{d}^p}{\mathrm{d}t^p}z_1. \tag{45}$$

As stated before, the polynomial on the left side is Hurwitz and with roots located sufficiently far away from the imaginary axis in the left half of the complex plane. Therefore, since $r^{(p)}(t)$ is bounded by assumption, the time response in (45) will be asymptotically, exponentially, ultimately bounded by a small disk centered around the origin of the error phase space, $e=\dot{e}=\cdots=e^{(p+1)}=0$. Moreover, the radius of the ultimate bounding disk is proportional to the inverse of the absolute value of the smallest real part of the roots of the characteristic polynomial (40). After (27) this means that the estimated values $\hat{x}_1$ and $\hat{x}_2$ can be made approximately close to the real values x_1 and x_2, respectively.

As a consequence of the convergence to an arbitrarily small neighborhood of zero of $e=\dot{e}=\cdots=e^{(p+1)}=0$, one can conclude after (42) that also $\tilde{z}_1$ can be made arbitrarily small, meaning that $\hat{z}_1$ becomes arbitrarily close to z_1. Note that this implies that the estimate of $\hat{x}_4$ given by (41) also becomes arbitrarily close to the actual value x_4. Finally, after (42), by computing the consecutive time derivatives of $\tilde{z}_1$, *i. e.*, $\tilde{z}^{(j)}$, the actual values $z^{(j)}$ are also approximately estimated via the corresponding observer vector variables, $\hat{z}_j(t)$, $j=1,2,\ldots$. See [15] for more details. $\triangle$

Remark 4.3.
It is rather trivial to design an observer for x_3 when x_4 is available just by changing (15)–(17) to

$$\dot{x}_1=x_2 \tag{46}$$
$$\dot{x}_2=z_1-\frac{A_2}{M}x_4-\frac{A_1-A_2}{M}p_{\text{atm}}-\frac{F_{\text{V}}}{M}x_2. \tag{47}$$

Note that as before (5) is not necessary since x_4 is measured, while x_3 is substituted by

$$z_1\overset{\triangle}{=}\frac{A_1}{M}x_3 \qquad\Rightarrow\qquad x_3=\frac{M}{A_1}z_1. \tag{48}$$

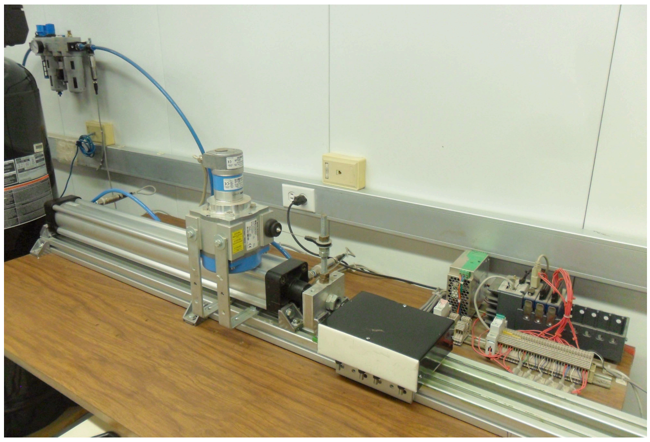

Fig. 2. Experimental test bed

The corresponding observer is then given by

$$\dot{\hat{x}}_1=\hat{x}_2+\lambda_{p+1}e-ae \tag{49}$$
$$\dot{\hat{x}}_2=\hat{z}_1-bx_4+\bar{u}-a\dot{\hat{x}}_1+\lambda_p e \tag{50}$$
$$\dot{\hat{z}}_1=\hat{z}_2+\lambda_{p-1}e \tag{51}$$
$$\dot{\hat{z}}_2=\hat{z}_3+\lambda_{p-2}e \tag{52}$$
$$\vdots$$
$$\dot{\hat{z}}_{p-1}=\hat{z}_p+\lambda_1 e \tag{53}$$
$$\dot{\hat{z}}_p=\lambda_0 e, \tag{54}$$

where this time $b=\frac{A_2}{M}$ and the estimated value of x_3 is

$$\hat{x}_3=\frac{M}{A_1}\hat{z}_1. \tag{55}$$

$\triangle$

5 Experimental results

To test the performance of the observers proposed in the last section, the device shown in Figure 2 will be employed. This is a *Telemecanique* actuator provided with a *Festo* proportional valve MYPE–5–1/8–HF–010 B, a *Festo* pressure sensor for each piston–chamber and the air supply, as well as a *Sick–Stegmann* absolute encoder for reading the piston position. It is controlled with a *CompactRio* acquisition system by *National Instruments* with a programmed sampling time of 2[ms] (fastest possible achievable). The air is distributed by an 230 liters air compressor *Craftsman Professional* and a *Festo* maintenance system with regulator. So as to be able to change the piston mass to introduce a perturbation, a box can be fixed at the piston–end as shown in Figure 2. This allows to increase the nominal mass up to in 50%. The following data has been used: $A_1=0.00316692174[\mathrm{m}^2]$, $A_2=0.00267604789[\mathrm{m}^2]$, $M=5.8[\mathrm{kg}]$, $F_{\text{V}}=150[(\mathrm{N}\cdot\mathrm{m})/\mathrm{s}]$ and $p_{\text{atm}}=0.9\cdot 10^5[\mathrm{Pa}]$

(for Mexico City). The interested reader can see [8] for details. No other system parameters are necessary for implementation. Finally, for both observers it was chosen $p = 3$ in (40), with the poles set to $s_1 = -20$, $s_2 = -20$, $s_3 = -40$, $s_4 = -60$ and $s_5 = -60$.

Remark 5.1. There is not an obvious way to choose the best value for p in (40) *a priori*. Theoretically, the larger the better. However, one can carry out an iterative procedure beginning with $p = 1$ and increasing its value until it does not represent any advantage, *i. e.* until the estimates given by the observer are similar for two consecutive values of p. On the other hand, usually $p = 3$ turns out to be a good choice. △

Remark 5.2. A disadvantage of the GPI method is that the transient performance may be very poor because of the presence of high peaks. In order to reduce this effect the so–called *clutch* can be implemented in the following form

$$\hat{\mathbf{x}}_{2s} = \begin{cases} \hat{\mathbf{x}}_2 \sin^8(\frac{\pi t}{2\varepsilon}), & 0 \le t \le \varepsilon \\ \hat{\mathbf{x}}_2, & t > \varepsilon \end{cases} \tag{56}$$

and

$$\hat{\mathbf{z}}_{is} = \begin{cases} \hat{\mathbf{z}}_i \sin^8(\frac{\pi t}{2\varepsilon}), & 0 \le t \le \varepsilon \\ \hat{\mathbf{z}}_i, & t > \varepsilon \end{cases} \quad i = 1, \ldots, p, \tag{57}$$

where $\hat{\mathbf{x}}_{2s}$ and $\hat{\mathbf{z}}_{is}, i = 1, \ldots, p$ are the softened versions of the observer's states and ε is the chosen *clutch*'s time. △

5.1 Comparative algorithm

In order to have a comparison point about the performance of the proposed algorithm, the well–known observer given in [10] is implemented too. Rewritten in the notation used in this paper, it is for the pressure p_1

$$\dot{\hat{x}}_1 = \hat{x}_2 + \alpha_1 \tilde{x}_1 + k_1 \mathrm{sign}(\tilde{x}_1) \tag{58}$$

$$\dot{\hat{x}}_2 = -\frac{F_v}{M}\hat{x}_2 + \frac{A}{M}\hat{p}_1 - \frac{A}{M}p_2 + \alpha_2 \tilde{x}_2 + k_2 \mathrm{sign}(\tilde{x}_2) \tag{59}$$

$$\dot{\hat{p}}_1 = -\kappa\frac{\hat{x}_2 \hat{p}_1}{x_1} + \frac{f_1 e_1}{h_1 x_1}u + \alpha_3 \tilde{x}_1 + \alpha_4 \tilde{x}_2 + k_3 \mathrm{sign}(\tilde{x}_1) + k_4 \mathrm{sign}(\tilde{x}_2) \tag{60}$$

and for p_2

$$\dot{\hat{x}}_1 = \hat{x}_2 + \alpha_1 \tilde{x}_1 + k_1 \mathrm{sign}(\tilde{x}_1) \tag{61}$$

$$\dot{\hat{x}}_2 = -\frac{F_v}{M}\hat{x}_2 + \frac{A}{M}p_1 - \frac{A}{M}\hat{p}_2 + \alpha_2 \tilde{x}_2 + k_2 \mathrm{sign}(\tilde{x}_2) \tag{62}$$

$$\dot{\hat{p}}_2 = \kappa\frac{\hat{x}_2 \hat{p}_2}{L - x_1} - \frac{f_2 e_2}{h_2(L - x_1)}u - \alpha_3 \tilde{x}_1 - \alpha_4 \tilde{x}_2 - k_3 \mathrm{sign}(\tilde{x}_1) - k_4 \mathrm{sign}(\tilde{x}_2), \tag{63}$$

where $\tilde{x}_1 = x_1 - \hat{x}_1$, $\tilde{x}_2 = x_2 - \hat{x}_2$, $k_1 = 0.2$, $k_2 = 10$, $k_3 = 20$, $k_4 = 1 \times 10^6$, $\alpha_1 = 100$, $\alpha_2 = 10$, $\alpha_3 = \alpha_4 = 10000$ are the observer's gains, $\kappa = 1.4$ is the ratio of specific heats, $A = 2.9214 \times 10^{-3}$[m^2] is the area of the chambers $f_1 = f_2 = 2.4062 \times 10^6$ (assuming sonic air flow through the valves), and $h_1 = h_2 = 1000$ and $e_1 = e_2 = 0.8192$ are the valve parameters.

5.2 Test signals and experimental cases

Six different input signals have been employed to test the robustness of the proposed approach under different circumstances. Recall that no control law is implemented since our goal is to test the observers. Thus, it is considered significative for the input both the frequency and the magnitude:

$$u_1(t) = 5 + 0.8\mathrm{square}(2\pi \cdot 0.1t) \text{ [V]} \tag{64}$$

$$u_2(t) = 5 + 1.0\mathrm{square}(2\pi \cdot 0.2t) \text{ [V]} \tag{65}$$

$$u_3(t) = 5 + 1.5\mathrm{square}(2\pi \cdot 2.0t) \text{ [V]} \tag{66}$$

$$u_4(t) = 5 + 2.0\sin(2\pi \cdot 0.3t) \text{ [V]} \tag{67}$$

$$u_5(t) = 5 + 2.5\sin(2\pi \cdot 0.5t) \text{ [V]} \tag{68}$$

$$u_6(t) = 5 + 3.0\sin(2\pi \cdot 2.0t) \text{ [V]}. \tag{69}$$

Also, each test signal has been used for three different cases

a) For the piston without any perturbation over the nominal parameters
b) An additional mass of $M_p = 2.9$[kg] is fixed on the piston (*i. e.* 50% of the nominal mass)
c) The additional mass is not fixed, but it is left at $x_p = 0.35$[m] so that the piston will hit and push it until it moves backwards. This represents an abrupt change in the moving mass

5.3 Outcomes for input $u_1(t)$

5.3.1 Without additional mass

For both schemes, the observers for x_3 and x_4 are implemented simultaneously since p_1 and p_2 are actually available and the estimated values are not used for feedback control. Figure 3 shows the outcomes. Since the units are MPa, even small relative errors turn out to be large in magnitude when expressed in Pa. Thus, so as to have a kind of percentual error $x_3 - \hat{x}_3$ is divided by x_3 and $x_4 - \hat{x}_4$ by x_4. Note that there are no units in this case. From Figure 3 it becomes clear that the proposed scheme GPI based Observer (GPIO) has a much better performance than the Sliding Mode based Observer (SMO). Although there are high peaks at the beginning, the errors tend very fast around zero. Note that the peaks would be even larger if the *clutch* mentioned in Remark 5.2 had not been implemented.

As to the piston position, the initial value of x_1 is 0.2[m] and it is set $\hat{x}_1(0) = 0$[m]. In Figure 4 it can be seen that the estimated variable tends rather fast to the real one, until $\tilde{x}_1$ oscillates around zero. To better appreciate this, the initial error of 200[mm] is not shown in the figure. The SMO

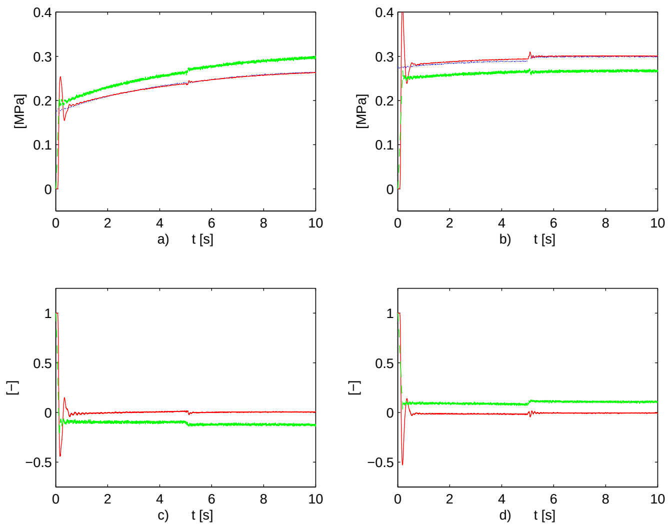

Fig. 3. Input $u_1(t)$ without additional mass. a) x_3 (···), $\hat{x}_3$ (—) with GPIO and $\hat{x}_3$ (- - -) with SMO. b) x_4 (···), $\hat{x}_4$ (—) with GPIO and $\hat{x}_4$ (- - -) with SMO. c) $(x_3 - \hat{x}_3)/x_3$, (—) with GPIO and (- - -) with SMO. d) $(x_4 - \hat{x}_4)/x_4$, (—) with GPIO and (- - -) with SMO.

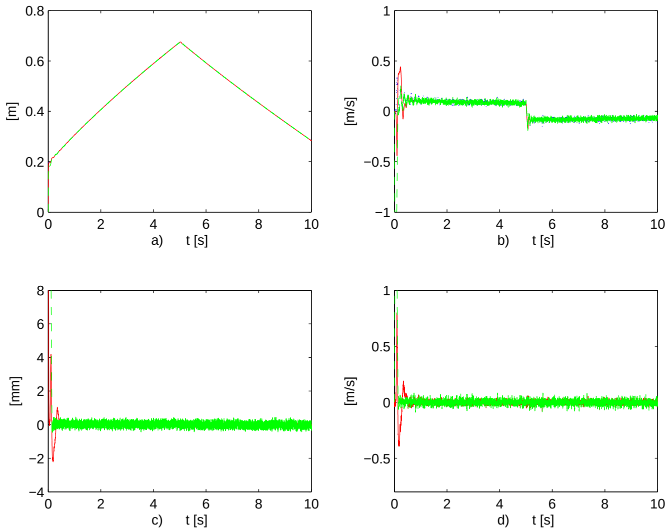

Fig. 4. Input $u_1(t)$ without additional mass. a) x_1 (···), $\hat{x}_1$ (—) with GPIO and $\hat{x}_1$ (- - -) with SMO. b) x_2 (···), $\hat{x}_2$ (—) with GPIO and $\hat{x}_2$ (- - -) with SMO. c) $x_1 - \hat{x}_1$, (—) with GPIO and (- - -) with SMO. d) $x_2 - \hat{x}_2$, (—) with GPIO and (- - -) with SMO.

delivers a similar position error for this case. Only the velocity x_2 may not be measured directly in our test bed, so that $\hat{x}_2$ can just be compared with an approximate value gotten by numerical differentiation and denoted by (making abuse of notation) as x_2 in Figure 4. It can be concluded that the performance of both observers was also accurate in this case.

5.3.2 With fixed additional mass

To test the robustness of the proposed observer in the presence of parameter uncertainties, an additional mass of 2.9[Kg] is added to the piston, *i. e.* 50% of the nominal

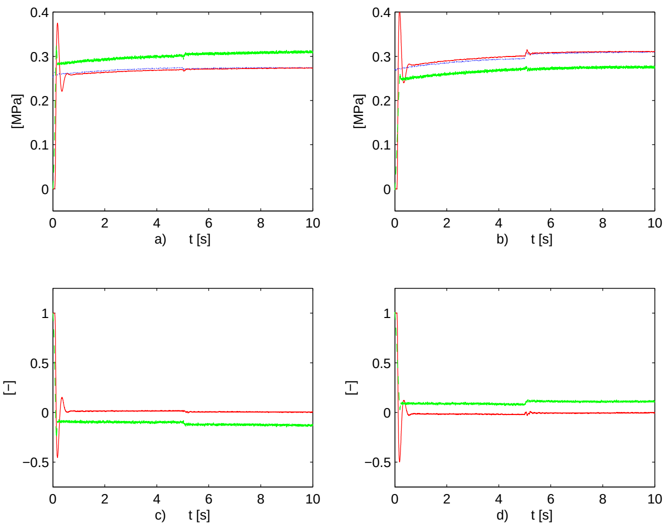

Fig. 5. Input $u_1(t)$ with fixed additional mass. a) x_3 (···), $\hat{x}_3$ (—) with GPIO and $\hat{x}_3$ (- - -) with SMO. b) x_4 (···), $\hat{x}_4$ (—) with GPIO and $\hat{x}_4$ (- - -) with SMO. c) $(x_3 - \hat{x}_3)/x_3$, (—) with GPIO and (- - -) with SMO. d) $(x_4 - \hat{x}_4)/x_4$, (—) with GPIO and (- - -) with SMO.

value. Note that an uncertainty of this kind introduces an error in many equations of the proposed observer and it is in some cases equivalent to an uncertainty on A_1 and/or on A_2, so that it is a quite important change (see for instance (17), (24)–(26) and (48)). The outcomes are shown in Figures 5 and 6. The experiment clearly shows a very good performance for such a large variation in the nominal mass, since the proposed observer was able to reconstruct the actual value almost as accurately as for the first case. On the other hand, the SMO shows pretty much the same behaviour as before too.

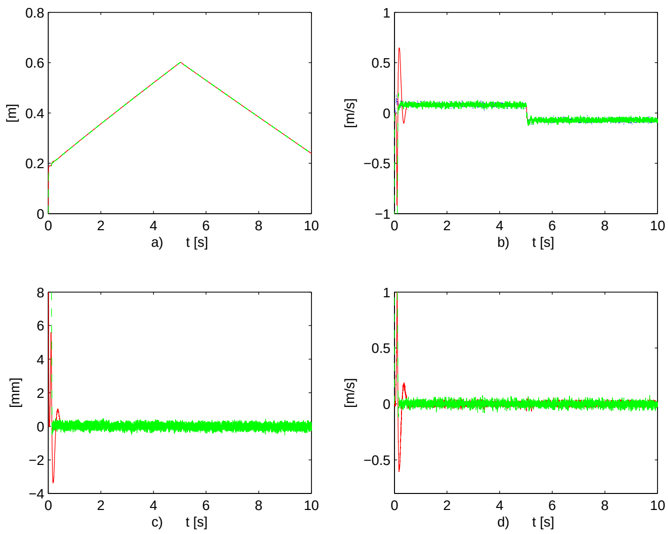

Fig. 6. Input $u_1(t)$ with fixed additional mass. a) x_1 (···), $\hat{x}_1$ (——) with GPIO and $\hat{x}_1$ (- - -) with SMO. b) x_2 (···), $\hat{x}_2$ (——) with GPIO and $\hat{x}_2$ (- - -) with SMO. c) $x_1 - \hat{x}_1$, (——) with GPIO and (- - -) with SMO. d) $x_2 - \hat{x}_2$, (——) with GPIO and (- - -) with SMO.

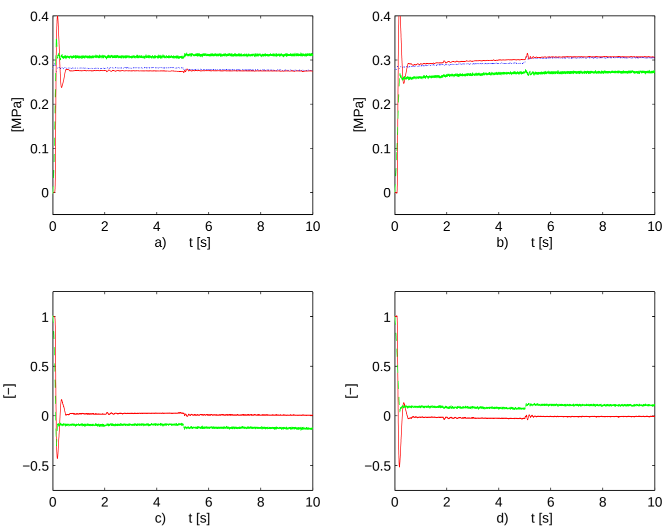

Fig. 7. Input $u_1(t)$ with not fixed additional mass. a) x_3 (···), $\hat{x}_3$ (——) with GPIO and $\hat{x}_3$ (- - -) with SMO. b) x_4 (···), $\hat{x}_4$ (——) with GPIO and $\hat{x}_4$ (- - -) with SMO. c) $(x_3 - \hat{x}_3)/x_3$, (——) with GPIO and (- - -) with SMO. d) $(x_4 - \hat{x}_4)/x_4$, (——) with GPIO and (- - -) with SMO.

5.3.3 With not fixed additional mass

Another kind of perturbation may be introduced whenever the piston mass changes suddenly. To achieve this goal, the extra mass is not fixed but placed at $x = 0.35$[m], so that it will be moved only as long as the piston pushes it. Once it begins its backwards movement the perturbation disappears for the rest of the experiment. The outcomes are shown in Figures 7 and 8. They are very similar to the case with the fixed mass even when the mass is changing. Thus, the variation on the errors is negligible regarding the previous cases. Note that the SMO is having also a similar performance as before.

5.4 Outcomes for input $u_2(t)$

Another way to test the robustness of the proposed scheme is by increasing the magnitude and the velocity of the input signal. For this goal are thought $u_2(t)$ and $u_3(t)$ in (65) and (66), respectively. In this section, the outcomes for $u_2(t)$ are presented, where the three experiments given in Section 5.3 are repeated. Figures 9 and 10 show the outcomes for the piston without additional mass. Note that the same scales as in Figures 3 and 4 are used, so as to have a more direct comparison. As before, when the square changes direction the errors suffer an increase which is slightly larger than for $u_1(t)$ and quite evidently twice more frequent. The same conclusions can be drawn when an extra mass is employed, both for the cases when it is fixed and when it is present only when the piston pushes it. The results can be seen in Figures 11 and 14.

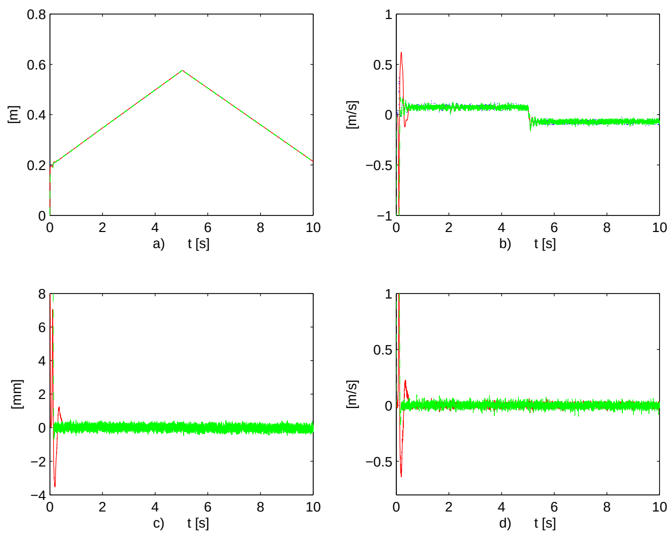

Fig. 8. Input $u_1(t)$ with not fixed additional mass. a) x_1 (···), $\hat{x}_1$ (——) with GPIO and $\hat{x}_1$ (- - -) with SMO. b) x_2 (···), $\hat{x}_2$ (——) with GPIO and $\hat{x}_2$ (- - -) with SMO. c) $x_1 - \hat{x}_1$, (——) with GPIO and (- - -) with SMO. d) $x_2 - \hat{x}_2$, (——) with GPIO and (- - -) with SMO.

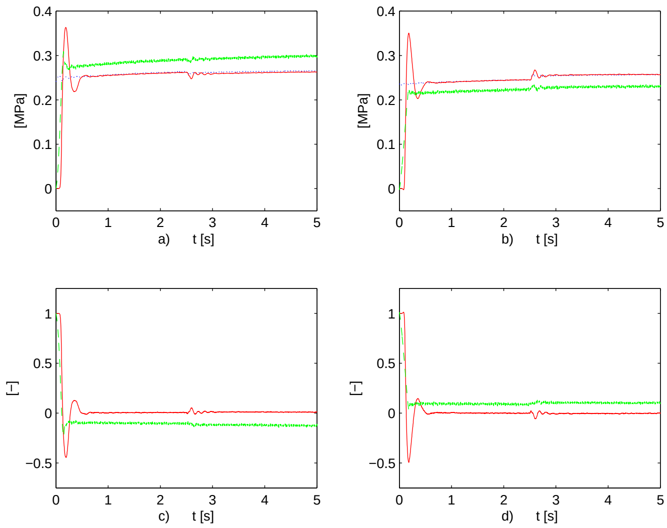

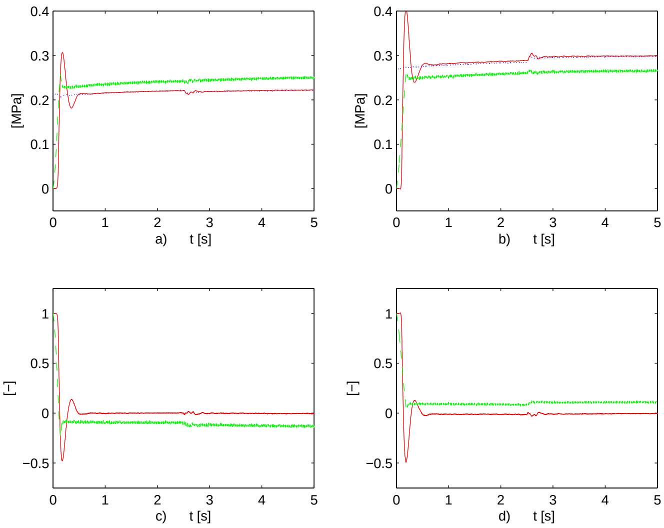

Fig. 9. Input $u_2(t)$ without additional mass. a) x_3 ($\cdots$), $\hat{x}_3$ (——) with GPIO and $\hat{x}_3$ (- - -) with SMO. b) x_4 ($\cdots$), $\hat{x}_4$ (——) with GPIO and $\hat{x}_4$ (- - -) with SMO. c) $(x_3 - \hat{x}_3)/x_3$, (——) with GPIO and (- - -) with SMO. d) $(x_4 - \hat{x}_4)/x_4$, (——) with GPIO and (- - -) with SMO.

Fig. 11. Input $u_2(t)$ with fixed additional mass. a) x_3 ($\cdots$), $\hat{x}_3$ (——) with GPIO and $\hat{x}_3$ (- - -) with SMO. b) x_4 ($\cdots$), $\hat{x}_4$ (——) with GPIO and $\hat{x}_4$ (- - -) with SMO. c) $(x_3 - \hat{x}_3)/x_3$, (——) with GPIO and (- - -) with SMO. d) $(x_4 - \hat{x}_4)/x_4$, (——) with GPIO and (- - -) with SMO.

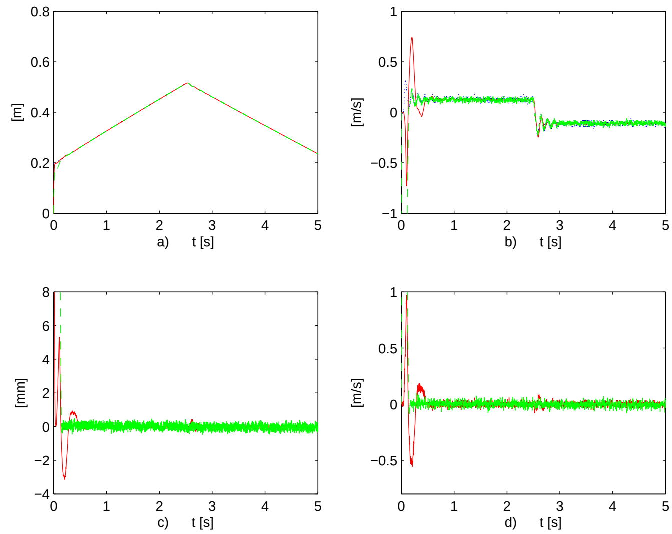

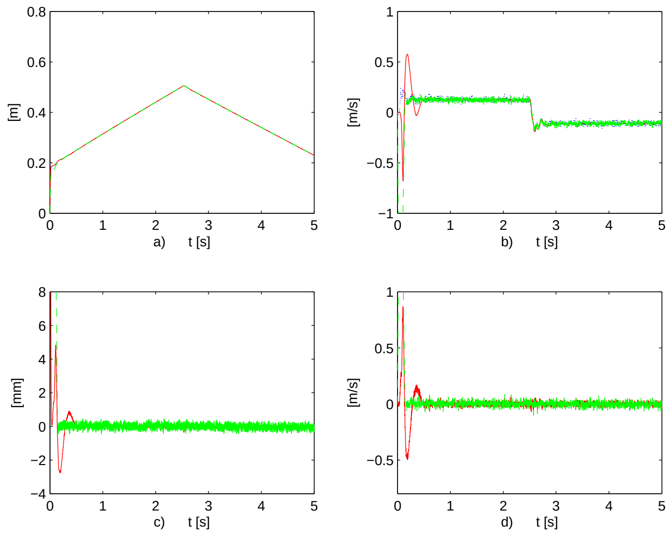

Fig. 10. Input $u_2(t)$ without additional mass. a) x_1 ($\cdots$), $\hat{x}_1$ (——) with GPIO and $\hat{x}_1$ (- - -) with SMO. b) x_2 ($\cdots$), $\hat{x}_2$ (——) with GPIO and $\hat{x}_2$ (- - -) with SMO. c) $x_1 - \hat{x}_1$, (——) with GPIO and (- - -) with SMO. d) $x_2 - \hat{x}_2$, (——) with GPIO and (- - -) with SMO.

Fig. 12. Input $u_2(t)$ with fixed additional mass. a) x_1 ($\cdots$), $\hat{x}_1$ (——) with GPIO and $\hat{x}_1$ (- - -) with SMO. b) x_2 ($\cdots$), $\hat{x}_2$ (——) with GPIO and $\hat{x}_2$ (- - -) with SMO. c) $x_1 - \hat{x}_1$, (——) with GPIO and (- - -) with SMO. d) $x_2 - \hat{x}_2$, (——) with GPIO and (- - -) with SMO.

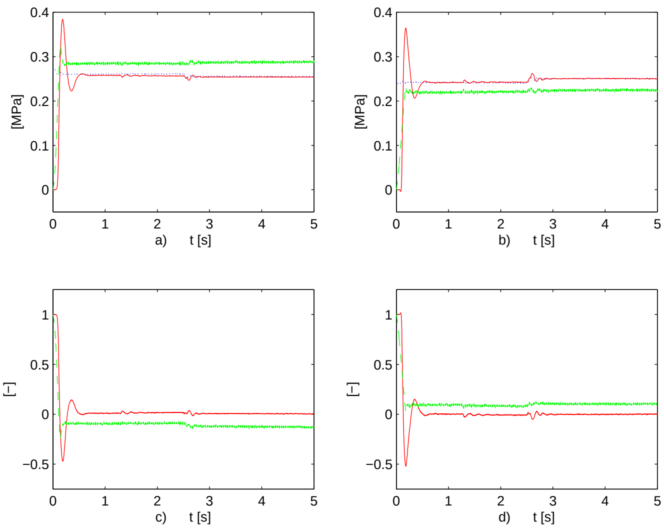

Fig. 13. Input $u_2(t)$ with not fixed additional mass. a) x_3 (···), $\hat{x}_3$ (——) with GPIO and $\hat{x}_3$ (- - -) with SMO. b) x_4 (···), $\hat{x}_4$ (——) with GPIO and $\hat{x}_4$ (- - -) with SMO. c) $(x_3 - \hat{x}_3)/x_3$, (——) with GPIO and (- - -) with SMO. d) $(x_4 - \hat{x}_4)/x_4$, (——) with GPIO and (- - -) with SMO.

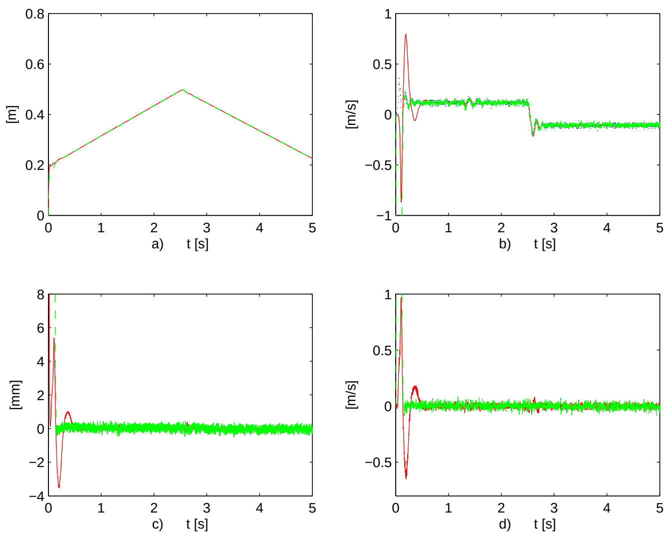

Fig. 14. Input $u_2(t)$ with not fixed additional mass. a) x_1 (···), $\hat{x}_1$ (——) with GPIO and $\hat{x}_1$ (- - -) with SMO. b) x_2 (···), $\hat{x}_2$ (——) with GPIO and $\hat{x}_2$ (- - -) with SMO. c) $x_1 - \hat{x}_1$, (——) with GPIO and (- - -) with SMO. d) $x_2 - \hat{x}_2$, (——) with GPIO and (- - -) with SMO.

5.5 Outcomes for input $u_3(t)$

For the input signal $u_3(t)$ the results are shown in Figures 15 to 20. As could have been expected, the errors became larger for both schemes. It also becomes rather clear that the high mass variation does not represent a key factor in the observer performance for any of the two schemes employed, while the input frequency does.

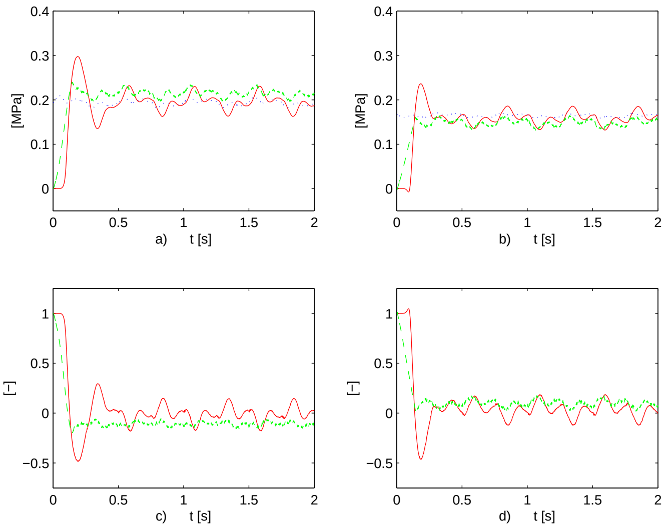

Fig. 15. Input $u_3(t)$ without additional mass. a) x_3 (···), $\hat{x}_3$ (——) with GPIO and $\hat{x}_3$ (- - -) with SMO. b) x_4 (···), $\hat{x}_4$ (——) with GPIO and $\hat{x}_4$ (- - -) with SMO. c) $(x_3 - \hat{x}_3)/x_3$, (——) with GPIO and (- - -) with SMO. d) $(x_4 - \hat{x}_4)/x_4$, (——) with GPIO and (- - -) with SMO.

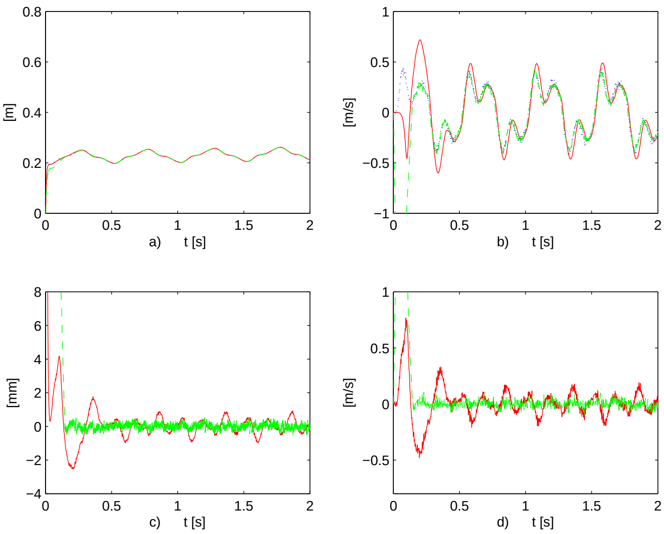

Fig. 16. Input $u_3(t)$ without additional mass. a) x_1 (···), $\hat{x}_1$ (——) with GPIO and $\hat{x}_1$ (- - -) with SMO. b) x_2 (···), $\hat{x}_2$ (——) with GPIO and $\hat{x}_2$ (- - -) with SMO. c) $x_1 - \hat{x}_1$, (——) with GPIO and (- - -) with SMO. d) $x_2 - \hat{x}_2$, (——) with GPIO and (- - -) with SMO.

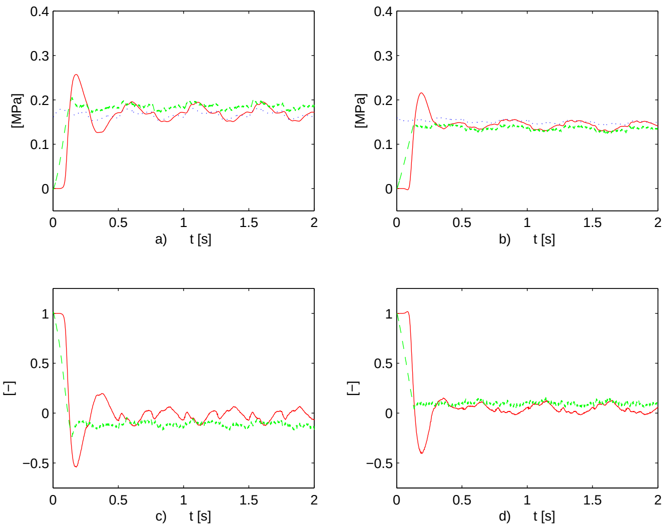

Fig. 17. Input $u_3(t)$ with fixed additional mass. a) x_3 ($\cdots$), $\hat{x}_3$ (——) with GPIO and $\hat{x}_3$ (- - -) with SMO. b) x_4 ($\cdots$), $\hat{x}_4$ (——) with GPIO and $\hat{x}_4$ (- - -) with SMO. c) $(x_3 - \hat{x}_3)/x_3$, (——) with GPIO and (- - -) with SMO. d) $(x_4 - \hat{x}_4)/x_4$, (——) with GPIO and (- - -) with SMO.

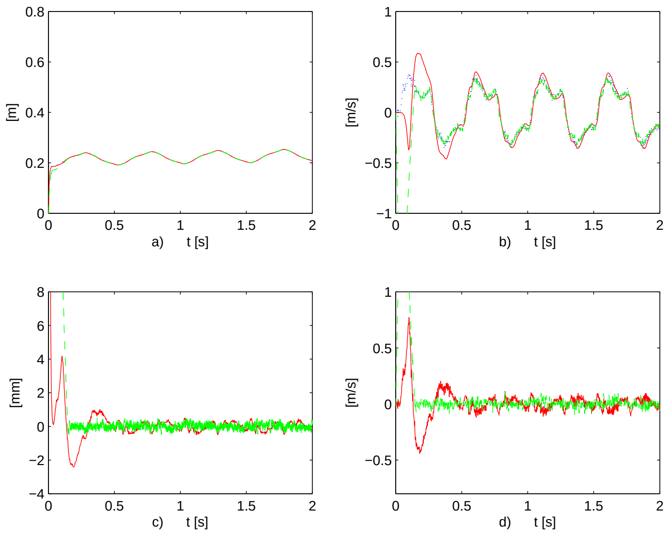

Fig. 18. Input $u_3(t)$ with fixed additional mass. a) x_1 ($\cdots$), $\hat{x}_1$ (——) with GPIO and $\hat{x}_1$ (- - -) with SMO. b) x_2 ($\cdots$), $\hat{x}_2$ (——) with GPIO and $\hat{x}_2$ (- - -) with SMO. c) $x_1 - \hat{x}_1$, (——) with GPIO and (- - -) with SMO. d) $x_2 - \hat{x}_2$, (——) with GPIO and (- - -) with SMO.

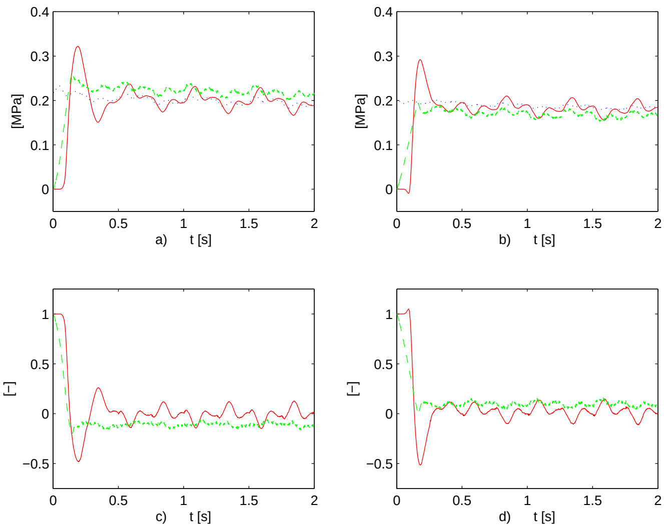

Fig. 19. Input $u_3(t)$ with not fixed additional mass. a) x_3 ($\cdots$), $\hat{x}_3$ (——) with GPIO and $\hat{x}_3$ (- - -) with SMO. b) x_4 ($\cdots$), $\hat{x}_4$ (——) with GPIO and $\hat{x}_4$ (- - -) with SMO. c) $(x_3 - \hat{x}_3)/x_3$, (——) with GPIO and (- - -) with SMO. d) $(x_4 - \hat{x}_4)/x_4$, (——) with GPIO and (- - -) with SMO.

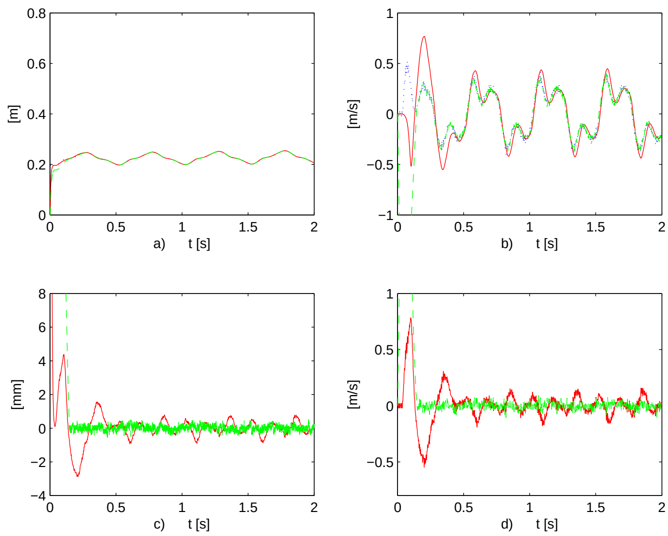

Fig. 20. Input $u_3(t)$ with not fixed additional mass. a) x_1 ($\cdots$), $\hat{x}_1$ (——) with GPIO and $\hat{x}_1$ (- - -) with SMO. b) x_2 ($\cdots$), $\hat{x}_2$ (——) with GPIO and $\hat{x}_2$ (- - -) with SMO. c) $x_1 - \hat{x}_1$, (——) with GPIO and (- - -) with SMO. d) $x_2 - \hat{x}_2$, (——) with GPIO and (- - -) with SMO.

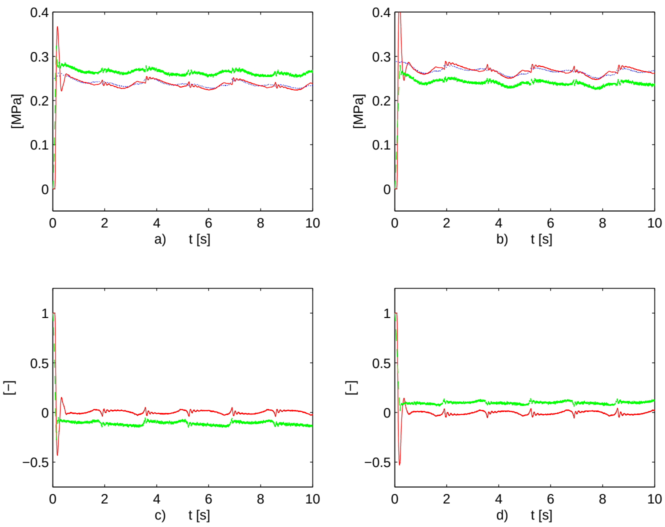

Fig. 21. Input $u_4(t)$ without additional mass. a) x_3 (···), $\hat{x}_3$ (——) with GPIO and $\hat{x}_3$ (- - -) with SMO. b) x_4 (···), $\hat{x}_4$ (——) with GPIO and $\hat{x}_4$ (- - -) with SMO. c) $(x_3 - \hat{x}_3)/x_3$, (——) with GPIO and (- - -) with SMO. d) $(x_4 - \hat{x}_4)/x_4$, (——) with GPIO and (- - -) with SMO.

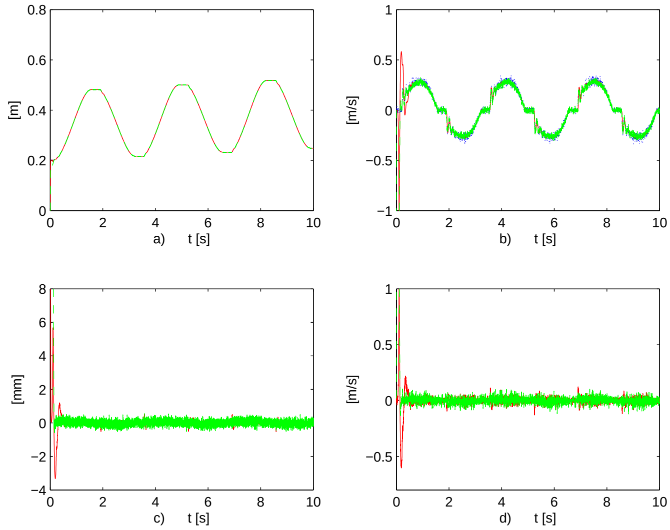

Fig. 22. Input $u_4(t)$ without additional mass. a) x_1 (···), $\hat{x}_1$ (——) with GPIO and $\hat{x}_1$ (- - -) with SMO. b) x_2 (···), $\hat{x}_2$ (——) with GPIO and $\hat{x}_2$ (- - -) with SMO. c) $x_1 - \hat{x}_1$, (——) with GPIO and (- - -) with SMO. d) $x_2 - \hat{x}_2$, (——) with GPIO and (- - -) with SMO.

5.6 Outcomes for input $u_4(t)$

The square waves change the movement direction abruptly and reflect the behaviour of the system for step inputs. It is therefore interesting to find out the observer performance for continuous input signals. For this goal, the sine waves $u_4(t)$ to $u_6(t)$ given in (67) to (69) are employed. As before, the frequency and the magnitude of each signal goes from the slowest to the fastest one. The outcomes for $u_4(t)$ are shown in Figures 21 to 26. As before, the proposed observer gets better results, while again the mass variation does not appear to represent any significative drawback.

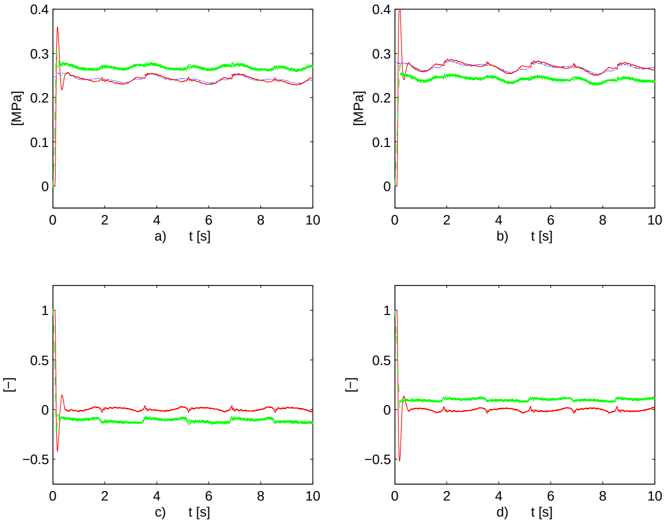

Fig. 23. Input $u_4(t)$ with fixed additional mass. a) x_3 (···), $\hat{x}_3$ (——) with GPIO and $\hat{x}_3$ (- - -) with SMO. b) x_4 (···), $\hat{x}_4$ (——) with GPIO and $\hat{x}_4$ (- - -) with SMO. c) $(x_3 - \hat{x}_3)/x_3$, (——) with GPIO and (- - -) with SMO. d) $(x_4 - \hat{x}_4)/x_4$, (——) with GPIO and (- - -) with SMO.

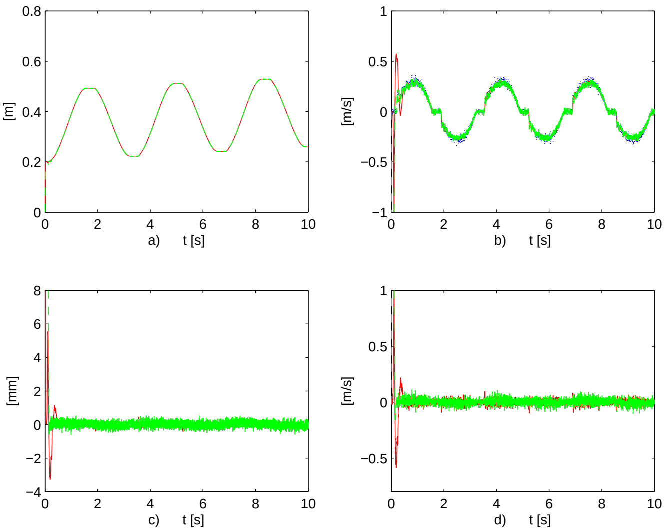

Fig. 24. Input $u_4(t)$ with fixed additional mass. a) x_1 (···), $\hat{x}_1$ (——) with GPIO and $\hat{x}_1$ (- - -) with SMO. b) x_2 (···), $\hat{x}_2$ (——) with GPIO and $\hat{x}_2$ (- - -) with SMO. c) $x_1 - \hat{x}_1$, (——) with GPIO and (- - -) with SMO. d) $x_2 - \hat{x}_2$, (——) with GPIO and (- - -) with SMO.

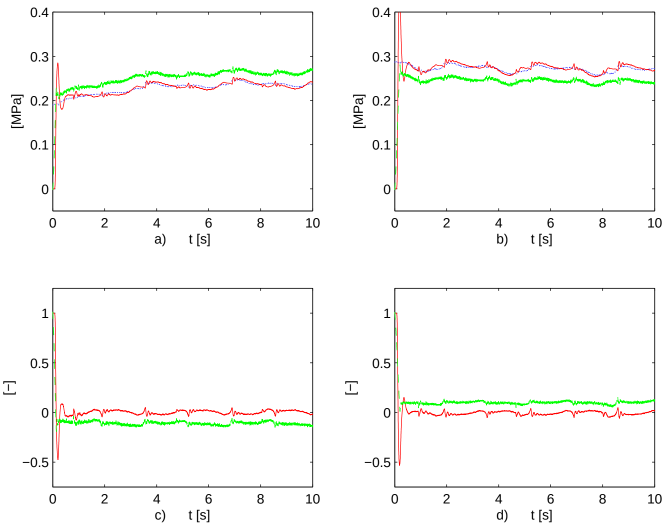

Fig. 25. Input $u_4(t)$ with not fixed additional mass. a) x_3 (···), $\hat{x}_3$ (—) with GPIO and $\hat{x}_3$ (- - -) with SMO. b) x_4 (···), $\hat{x}_4$ (—) with GPIO and $\hat{x}_4$ (- - -) with SMO. c) $(x_3 - \hat{x}_3)/x_3$, (—) with GPIO and (- - -) with SMO. d) $(x_4 - \hat{x}_4)/x_4$, (—) with GPIO and (- - -) with SMO.

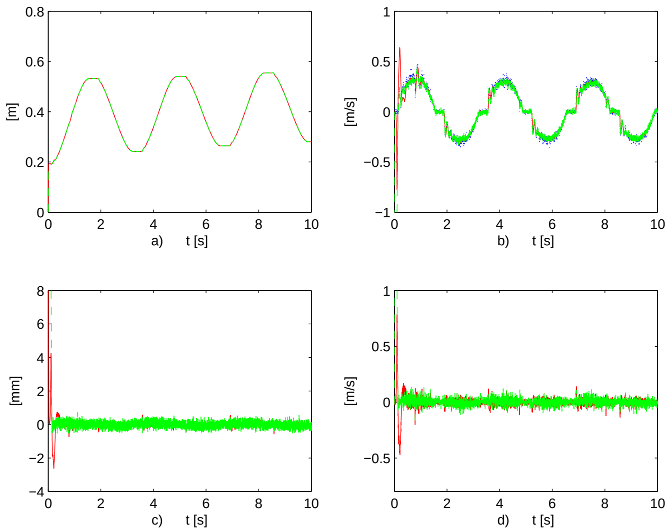

Fig. 26. Input $u_4(t)$ with not fixed additional mass. a) x_1 (···), $\hat{x}_1$ (—) with GPIO and $\hat{x}_1$ (- - -) with SMO. b) x_2 (···), $\hat{x}_2$ (—) with GPIO and $\hat{x}_2$ (- - -) with SMO. c) $x_1 - \hat{x}_1$, (—) with GPIO and (- - -) with SMO. d) $x_2 - \hat{x}_2$, (—) with GPIO and (- - -) with SMO.

5.7 Outcomes for input $u_5(t)$

The sine wave in (68) is larger in magnitude and frequency than that given in (67). The outcomes can be seen in Figures 27 to 32. It can be appreciated that the results for both schemes are similar. The disadvantage of the GPIO lacks as usual in the transient performance. Once again, the high variation in the mass has a relative small effect on the performance of both observers.

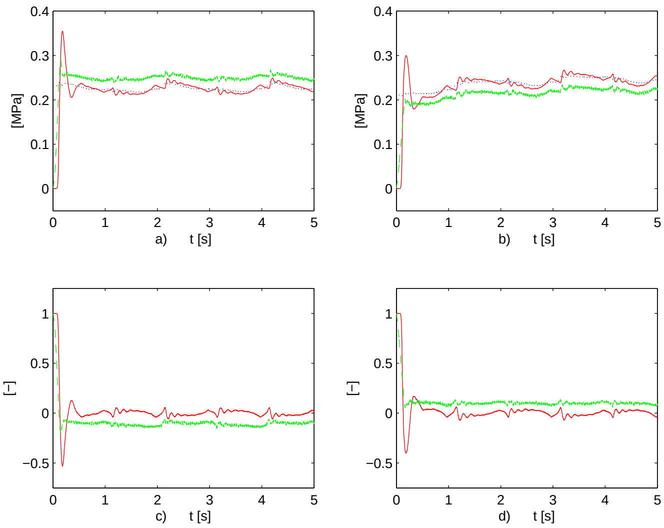

Fig. 27. Input $u_5(t)$ without additional mass. a) x_3 (···), $\hat{x}_3$ (—) with GPIO and $\hat{x}_3$ (- - -) with SMO. b) x_4 (···), $\hat{x}_4$ (—) with GPIO and $\hat{x}_4$ (- - -) with SMO. c) $(x_3 - \hat{x}_3)/x_3$, (—) with GPIO and (- - -) with SMO. d) $(x_4 - \hat{x}_4)/x_4$, (—) with GPIO and (- - -) with SMO.

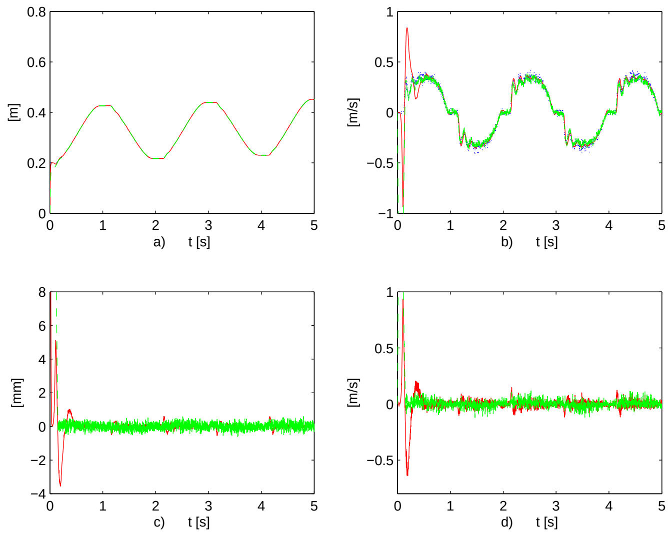

Fig. 28. Input $u_5(t)$ without additional mass. a) x_1 (···), $\hat{x}_1$ (—) with GPIO and $\hat{x}_1$ (- - -) with SMO. b) x_2 (···), $\hat{x}_2$ (—) with GPIO and $\hat{x}_2$ (- - -) with SMO. c) $x_1 - \hat{x}_1$, (—) with GPIO and (- - -) with SMO. d) $x_2 - \hat{x}_2$, (—) with GPIO and (- - -) with SMO.

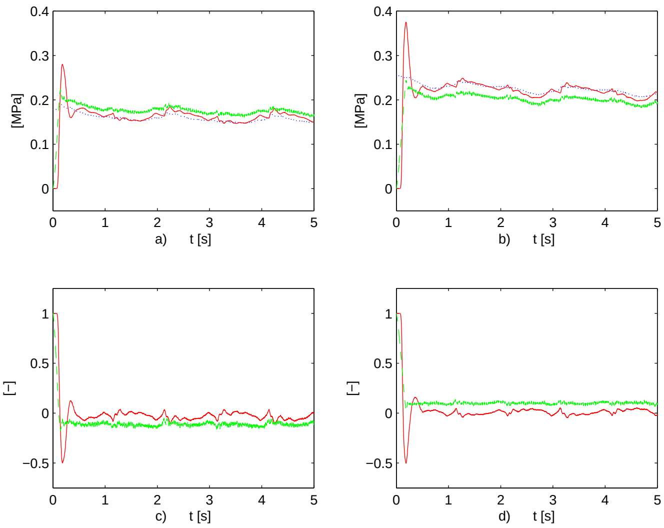

Fig. 29. Input $u_5(t)$ with fixed additional mass. a) x_3 ($\cdots$), $\hat{x}_3$ (——) with GPIO and $\hat{x}_3$ (- - -) with SMO. b) x_4 ($\cdots$), $\hat{x}_4$ (——) with GPIO and $\hat{x}_4$ (- - -) with SMO. c) $(x_3 - \hat{x}_3)/x_3$, (——) with GPIO and (- - -) with SMO. d) $(x_4 - \hat{x}_4)/x_4$, (——) with GPIO and (- - -) with SMO.

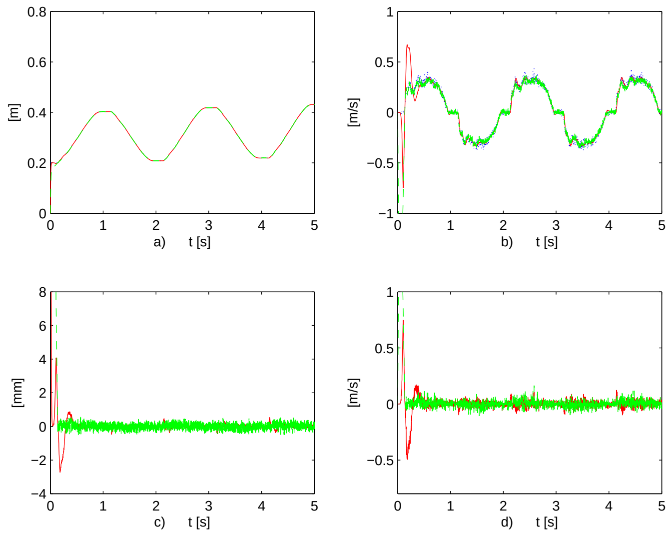

Fig. 30. Input $u_5(t)$ with fixed additional mass. a) x_1 ($\cdots$), $\hat{x}_1$ (——) with GPIO and $\hat{x}_1$ (- - -) with SMO. b) x_2 ($\cdots$), $\hat{x}_2$ (——) with GPIO and $\hat{x}_2$ (- - -) with SMO. c) $x_1 - \hat{x}_1$, (——) with GPIO and (- - -) with SMO. d) $x_2 - \hat{x}_2$, (——) with GPIO and (- - -) with SMO.

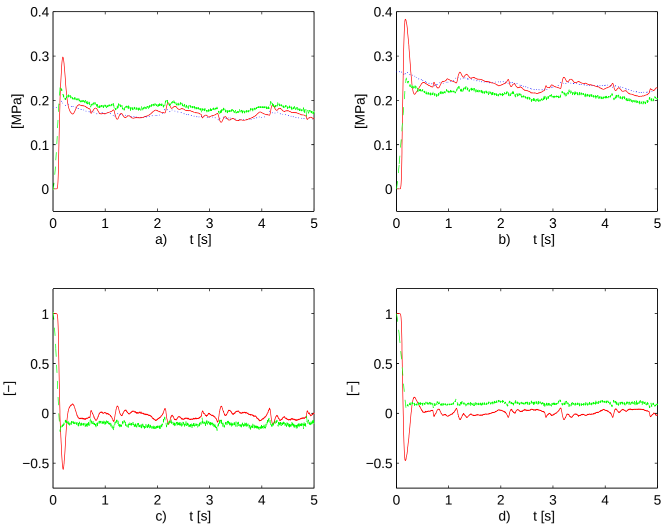

Fig. 31. Input $u_5(t)$ with not fixed additional mass. a) x_3 ($\cdots$), $\hat{x}_3$ (——) with GPIO and $\hat{x}_3$ (- - -) with SMO. b) x_4 ($\cdots$), $\hat{x}_4$ (——) with GPIO and $\hat{x}_4$ (- - -) with SMO. c) $(x_3 - \hat{x}_3)/x_3$, (——) with GPIO and (- - -) with SMO. d) $(x_4 - \hat{x}_4)/x_4$, (——) with GPIO and (- - -) with SMO.

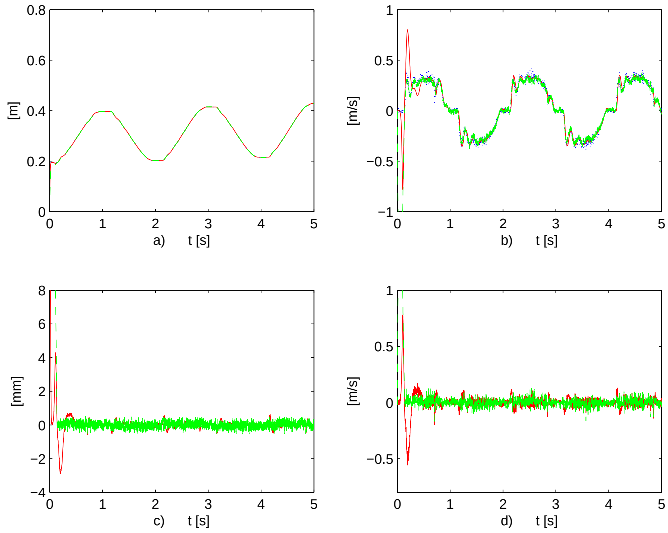

Fig. 32. Input $u_5(t)$ with not fixed additional mass. a) x_1 ($\cdots$), $\hat{x}_1$ (——) with GPIO and $\hat{x}_1$ (- - -) with SMO. b) x_2 ($\cdots$), $\hat{x}_2$ (——) with GPIO and $\hat{x}_2$ (- - -) with SMO. c) $x_1 - \hat{x}_1$, (——) with GPIO and (- - -) with SMO. d) $x_2 - \hat{x}_2$, (——) with GPIO and (- - -) with SMO.

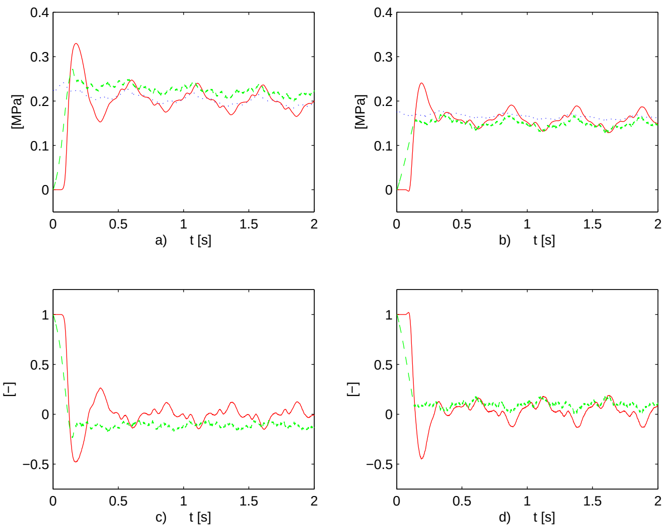

Fig. 33. Input $u_6(t)$ without additional mass. a) x_3 ($\cdots$), $\hat{x}_3$ (—) with GPIO and $\hat{x}_3$ (- - -) with SMO. b) x_4 ($\cdots$), $\hat{x}_4$ (—) with GPIO and $\hat{x}_4$ (- - -) with SMO. c) $(x_3 - \hat{x}_3)/x_3$, (—) with GPIO and (- - -) with SMO. d) $(x_4 - \hat{x}_4)/x_4$, (—) with GPIO and (- - -) with SMO.

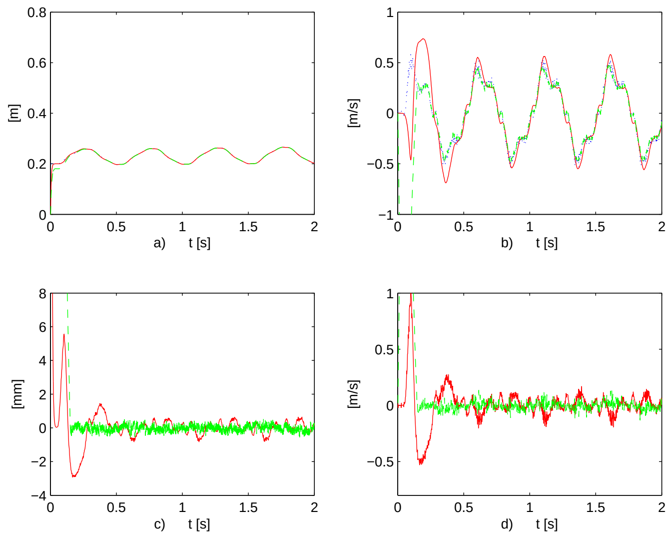

Fig. 34. Input $u_6(t)$ without additional mass. a) x_1 ($\cdots$), $\hat{x}_1$ (—) with GPIO and $\hat{x}_1$ (- - -) with SMO. b) x_2 ($\cdots$), $\hat{x}_2$ (—) with GPIO and $\hat{x}_2$ (- - -) with SMO. c) $x_1 - \hat{x}_1$, (—) with GPIO and (- - -) with SMO. d) $x_2 - \hat{x}_2$, (—) with GPIO and (- - -) with SMO.

5.8 Outcomes for input $u_6(t)$

The fasted sine wave is used here. The results can be seen in Figures 33 to 38. The experiment shows even clearer that the proposed scheme performance becomes poorer for high velocities. At the same time, for the SMO the increase in the pressure error estimation is more moderate while it is higher for the position estimation. For short, both schemes are more sensitive to high frequencies than to mass variations.

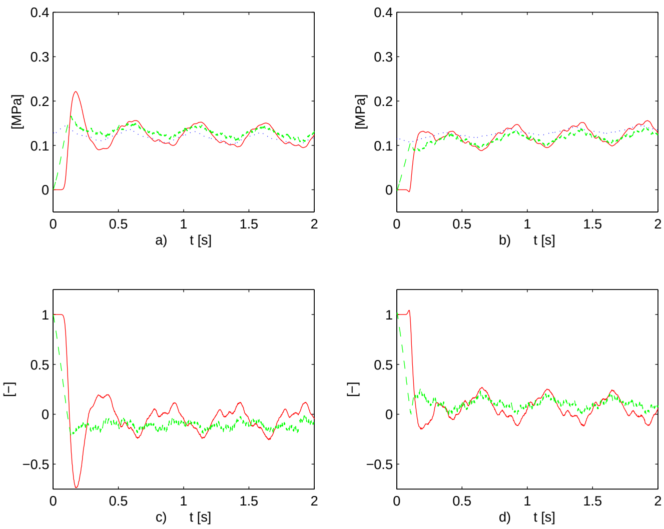

Fig. 35. Input $u_6(t)$ with fixed additional mass. a) x_3 ($\cdots$), $\hat{x}_3$ (—) with GPIO and $\hat{x}_3$ (- - -) with SMO. b) x_4 ($\cdots$), $\hat{x}_4$ (—) with GPIO and $\hat{x}_4$ (- - -) with SMO. c) $(x_3 - \hat{x}_3)/x_3$, (—) with GPIO and (- - -) with SMO. d) $(x_4 - \hat{x}_4)/x_4$, (—) with GPIO and (- - -) with SMO.

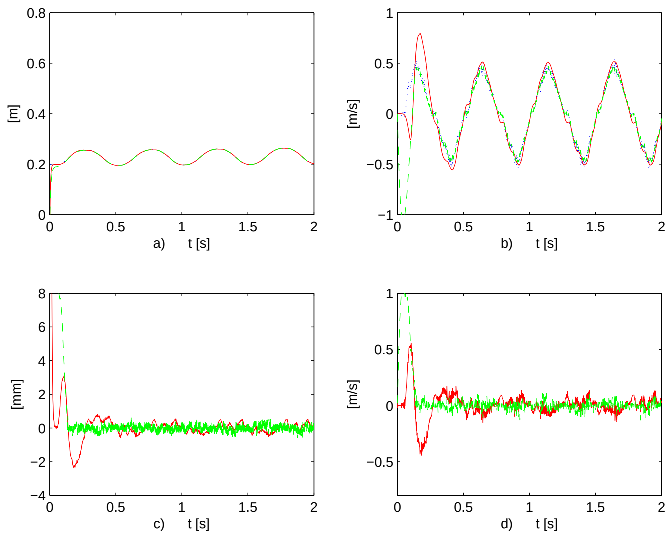

Fig. 36. Input $u_6(t)$ with fixed additional mass. a) x_1 ($\cdots$), $\hat{x}_1$ (—) with GPIO and $\hat{x}_1$ (- - -) with SMO. b) x_2 ($\cdots$), $\hat{x}_2$ (—) with GPIO and $\hat{x}_2$ (- - -) with SMO. c) $x_1 - \hat{x}_1$, (—) with GPIO and (- - -) with SMO. d) $x_2 - \hat{x}_2$, (—) with GPIO and (- - -) with SMO.

5.9 Discussion

The experimental results clearly show a good performance of the GPIO for low and medium input velocities and that it owns strong robustness properties against high mass variations. However, it diminishes its performance when the input signal increases in frequency and magnitude. This effect was observed consistently with sine and square waves as inputs. There are two possible reasons for this behaviour. On the one hand, friction effects do depend on the velocity x_2. Thus, its influence will be stronger for higher velocities. Our approach assumes that the only perturbation present in model (3) is either x_3 or x_4, while there is only viscous fric-

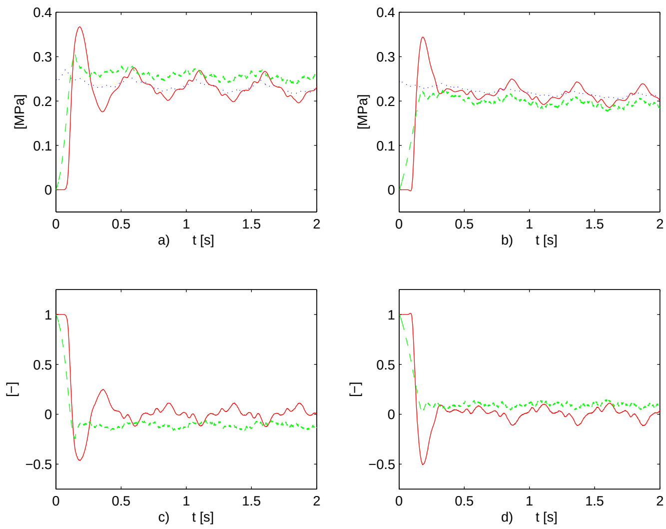

Fig. 37. Input $u_6(t)$ with not fixed additional mass. a) x_3 ($\cdots$), $\hat{x}_3$ (—) with GPIO and $\hat{x}_3$ (- - -) with SMO. b) x_4 ($\cdots$), $\hat{x}_4$ (—) with GPIO and $\hat{x}_4$ (- - -) with SMO. c) $(x_3-\hat{x}_3)/x_3$, (—) with GPIO and (- - -) with SMO. d) $(x_4-\hat{x}_4)/x_4$, (—) with GPIO and (- - -) with SMO.

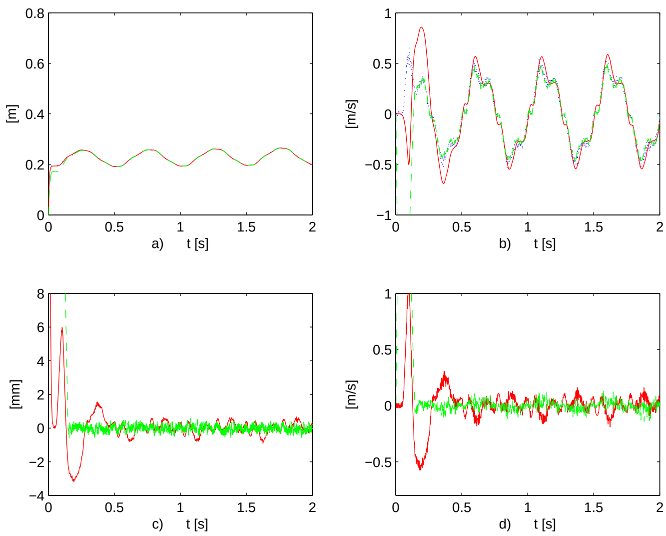

Fig. 38. Input $u_6(t)$ with not fixed additional mass. a) x_1 ($\cdots$), $\hat{x}_1$ (—) with GPIO and $\hat{x}_1$ (- - -) with SMO. b) x_2 ($\cdots$), $\hat{x}_2$ (—) with GPIO and $\hat{x}_2$ (- - -) with SMO. c) $x_1-\hat{x}_1$, (—) with GPIO and (- - -) with SMO. d) $x_2-\hat{x}_2$, (—) with GPIO and (- - -) with SMO.

tion present. Therefore, nonlinear friction effects may rise for high frequencies and will become undistinguishable from the unknown pressure, thus making its reconstruction less accurate. On the other hand, the GPIO is based on high gains and setting poles with high magnitudes, making it more sensitive to the process of discretization. It may turn out that a sampling time of 2[ms] is not fast enough. Finally, the SMO chosen for comparison purposes is more robust than the proposed algorithm to estimate the unknown pressures in the sense that the errors do not increase its magnitude as much as it does for the GPIO. However, the performance for

Table 2. RMSE for $(x_3-\hat{x}_3)/x_3$

In	GPIO NAM	SMO NAM	GPIO FAM	SMO FAM	GPIO NFAM	SMO NFAM
u_1	0.109	0.129	0.110	0.132	0.110	0.131
u_2	0.153	0.150	0.155	0.148	0.154	0.150
u_3	0.255	0.190	0.253	0.191	0.250	0.193
u_4	0.110	0.131	0.110	0.133	0.112	0.129
u_5	0.159	0.148	0.163	0.148	0.163	0.148
u_6	0.253	0.194	0.283	0.180	0.251	0.195

Table 3. RMSE for $(x_4-\hat{x}_4)/x_4$

In	GPIO NAM	SMO NAM	GPIO FAM	SMO FAM	GPIO NFAM	SMO NFAM
u_1	0.113	0.130	0.112	0.131	0.114	0.129
u_2	0.159	0.152	0.158	0.155	0.161	0.150
u_3	0.264	0.191	0.254	0.185	0.261	0.196
u_4	0.113	0.130	0.113	0.131	0.114	0.131
u_5	0.156	0.147	0.159	0.153	0.159	0.155
u_6	0.263	0.191	0.265	0.183	0.257	0.204

low frequencies is clearly poorer, for medium frequencies is similar and just for high input frequencies is better.

In order to have another insight about the experimental outcomes, the RMSE index employed in [2, 8] and given by

$$\mathrm{RMSE} = \sqrt{\frac{1}{n}\sum_{i=1}^{n} e_i^2} \tag{70}$$

is also used in this work. In (70), i is the current sample number, e_i is the corresponding error and n is the total number of samples. The results for the pressure estimation can be seen in Tables 2 and 3, where NAM = No Additional Mass, FAM = Fixed Additional Mass, and NFAM = Not Fixed Additional Mass. From the tables the same conclusions can be inferred. In Tables 4 and 5 the RMSE indexes for position and velocity errors are shown, respectively. Most interesting, the GPIO is better for all cases, regardless the input frequency. Note that the SMO also shows peaks during the transient response, what increases the RMSE. This means that the GPIO shows a higher performance altogether.

Table 4. RMSE for $(x_1 - \hat{x}_1)$ [mm]

In	GPIO NAM	SMO NAM	GPIO FAM	SMO FAM	GPIO NFAM	SMO NFAM
u_1	3.673	4.825	3.563	5.004	3.685	5.269
u_2	5.258	7.307	4.957	6.693	5.188	7.304
u_3	8.150	10.948	7.785	10.265	8.236	11.214
u_4	3.786	5.233	3.766	5.221	3.648	4.839
u_5	5.303	7.208	5.299	6.964	5.158	6.841
u_6	8.395	11.448	8.311	10.647	8.121	11.367

Table 5. RMSE for $(x_2 - \hat{x}_2)$ [m/s]

In	GPIO NAM	SMO NAM	GPIO FAM	SMO FAM	GPIO NFAM	SMO NFAM
u_1	0.056	0.139	0.077	0.226	0.085	0.254
u_2	0.104	0.314	0.091	0.246	0.108	0.333
u_3	0.159	0.394	0.132	0.314	0.162	0.438
u_4	0.077	0.218	0.074	0.221	0.061	0.153
u_5	0.102	0.275	0.081	0.199	0.086	0.216
u_6	0.172	0.451	0.116	0.201	0.187	0.512

6 Conclusions

In this paper, an observability analysis for differential pneumatic pistons is presented. It is shown that the system will be observable as long as the piston position and the pressure of any chamber is measured. Linear observers are designed and implemented based on the GPI (*Generalized Proportional Integral*) approach. This strategy is chosen because of the scarce information of the system model necessary for implementation. To test the proposed algorithm in performance and robustness a complete set of experiments is carried out and the results compared with a well–known Sliding Mode based Observer (SMO). The outcomes clearly show a very good and robust performance of the proposed scheme for low and medium input velocities and superior to the SMO. Only for very high input velocities the observer performance decreases.

Achnowledgements

This work is based on research supported by the **DGAPA–UNAM** under grant **IN116314**.

References

[1] Ning, S., and Bone, G. M., 2002. "High steady-state accuracy pneumatic servo positioning system with PVA/PV control and friction compensation". In Proceedings of the IEEE International Conference on Robotics and Automation, Washington, DC.

[2] Ning, S., and Bone, G. M., 2005. "Experimental comparison of two pneumatic servo position control algorithms". In Proceedings of the IEEE International Conference on Mechatronics and Automation, Niagara Falls, Canada.

[3] Sawodny, O., and Hildebrandt, A., 2002. "Aspects of the control of differential pneumatic cylinders". In 10th German Japanese Seminar on Problems in Dynamical Systems, Kanazawa.

[4] Shen, X., Zhang, J., Barth, E. J., and Goldfarb, M., 2006. "Nonlinear model-based contrl of pulse width modulated pneumatic servo systems". *ASME Journal of Dynamic Systems, Measurement, and Control*, **128**, pp. 663–669.

[5] Guenther, R., Perondi, E. A., DePieri, E. R., and Valdiero, A. C., 2006. "Cascade controlled pneumatic positioning system with LuGre model based friction compensation". *Journal of the Brazilien Society of Mechanic Science and Engineering*, **28**(1), January–March, pp. 48–57.

[6] Zhu, Y., 2006. *Control of pneumatic systems for free space and interaction tasks with system and environmental uncertainties*. Dissertation, School of Vanderbilt University, Nashville, Tennessee, United Staates of America.

[7] Goettert, M., and Neumann, R., 2007. "Bahnregelung servopneumatischer Antriebe - ein Vergleich von linearen und nichtlinearen Reglern". *Autmoatisierungs Technik*, **2**, pp. 69–74.

[8] Weist, J., Arteaga Pérez, M. A., de la Cruz, L. R., and Hebisch, H., 2011. "Model free control for differential pneumatic pistons: Experimental comparison". *International Journal of Control*, **84**(1), pp. 138–164.

[9] Bigras, P., and Khayati, K., 2002. "Nonlinear observer for pneumatic system with non negligible connection port restriction". In Proc. American Control Conference, pp. 3191–3195.

[10] Pandian, S. R., Takemura, F., Hayakawa, Y., and Kawamura, S., 2002. "Pressure observer–controller design for pneumatic cylinder actuators". *IEEE/ASME Transactions on Mechatronics*, **7**(4), pp. 490–499.

[11] Wu, J., Goldfarb, M., and Barth, E., 2003. "The role of pressure sensors in the servo control of pneumatic actuators". In Proc. American Control Conference, Vol. 2, pp. 1710–1714.

[12] Wu, J., Goldfarb, M., and Barth, E., 2004. "On the observability of pressure in a pneumatic servo actuator". *ASME Journal of Dynamic Systems, Measurement, and Control*, **126**, December, pp. 921–924.

[13] Gulati, N., and Barth, E. J., 2005. "Non–linear pressure observer design for pneumatic actuators". In Proceedings of the 2005 IEEE/ASME International Conference

on Advanced Intelligent Mechatronics, pp. 783–788.

[14] Fliess, M., Marquez, R., Delaleau, E., and Sira-Ramírez, H., 2002. "Correcteurs proportionnels intègraux généralisés". *ESAIM: Control, Optimisation and Calculus of Variations*, **7**(2), pp. 23–41.

[15] Sira-Ramírez, H., Ramírez-Neria, M., and Rodríguez-Ángeles, A., 2010. "On the linear control of nonlinear mechanical systems". In Proc. of 49th IEEE Conference on Decision and Control, pp. 1999–2004.

[16] Goettert, M., and Neumann, R., 1999. "Nichtlineare Regelungskonzepte für servopneumatische Roboter". In Proceedings 3. Deutsch-Polnisches Seminar Inovation und Fortschritt in der Fluidtechnik, Zakopane, Poland.

[17] Sobczyk, M. R., and Perondi, E. A., 2006. "Variable structure cascade control of a pneumatic positioning system". *ABCM Symposium Series in Mechatronics*, **2**, pp. 27–34.

[18] Beater, P., 2007. *Pneumatic Drives*. Springer-Verlag Berlin Heidelberg.

[19] Diop, S., and Fliess, M., 1991. "Nonlinear observability, identifiability and persistent trajectories". In Proc. of the 36th IEEE Conference on Decision and Control.

[20] Hermann, R., and Krener, A. J., 1977. "Nonlinear controllability and observability". *IEEE Transactions on Automatic Control*, **22**(5), pp. 728–740.